Studies in Conservation

ISSN: 0039-3630 (Print) 2047-0584 (Online) Journal homepage: https://www.tandfonline.com/loi/ysic20

The Influence of Relative Humidity and Intrinsic Chloride on Post-excavation Corrosion Rates of Archaeological Wrought Iron

David E. Watkinson, Melanie B. Rimmer & Nicola J. Emmerson

To cite this article: David E. Watkinson, Melanie B. Rimmer & Nicola J. Emmerson (2019) The Influence of Relative Humidity and Intrinsic Chloride on Post-excavation Corrosion Rates of Archaeological Wrought Iron, Studies in Conservation, 64:8, 456-471, DOI: 10.1080/00393630.2018.1565006

To link to this article: https://doi.org/10.1080/00393630.2018.1565006

Published online: 08 Feb 2019.

STUDIES IN CONSERVATION
2019, VOL. 64, NO. 8, 456–471
https://doi.org/10.1080/00393630.2018.1565006

ORIGINAL RESEARCH OR TREATMENT PAPER

OPEN ACCESS Check for updates

The Influence of Relative Humidity and Intrinsic Chloride on Post-excavation Corrosion Rates of Archaeological Wrought Iron

David E. Watkinson, Melanie B. Rimmer and Nicola J. Emmerson

Department of Archaeology & Conservation, School of History, Archaeology & Religion, Cardiff University, Cardiff, UK

ABSTRACT

This study examined the impact of relative humidity (RH) on the corrosion rate of 129 archaeological iron nails from two sites. Oxygen consumption of individual nails in controlled RH was used as a corrosion rate proxy to deliver quantitative data on corrosion rate as a function of RH. This was negligible at 20% RH, slow up to 40% RH for both sites, and increased rapidly at 60% RH for Roman nails from Caerleon (Wales) and at 70% RH for medieval nails from Billingsgate (London). The nails were digested and their chloride content was determined and related to their oxygen consumption at specific RH values. While a generic pattern of corrosion as a function of chloride was identified, for any single concentration of chloride corrosion rate was not predictable. Desiccation is in common use to control post-excavation corrosion of archaeological iron; quantifying how differing levels of desiccation changed corrosion rate provided a scaled tool for identifying corrosion risk, estimating object longevity, and calculating cost benefit for storage options.

ARTICLE HISTORY
Received October 2018
Accepted December 2018

KEYWORDS
Iron; corrosion; archaeological; storage; display; relative humidity; desiccation; management

Introduction

Context of the study

The occurrence and control of the post-excavation corrosion of archaeological iron present major challenges for professionals involved in the preservation of heritage. While conservators recognise that the chloride ions (Cl^-) within excavated objects, oxygen, and atmospheric moisture play a major role in determining the corrosion rate of archaeological iron, there remains no published information quantifying their impact. Treatment design largely relies upon the concept that oxygen is required for corrosion to occur and increasing ambient RH and the Cl^- concentration within objects increases corrosion rate. Extensive research published in corrosion science contexts on the influence of aqueous solutions, relative humidity (RH), and Cl^- concentration on corrosion rates of modern steels is of limited use for determining the corrosion rates of extensively corroded and Cl^- contaminated archaeological iron. The use of experimentally generated quantitative data to identify the parameters that will maximise the operational lifespan of modern ferrous alloys within industrial, engineering, and commercial contexts is a concept that can be adapted within heritage studies to underpin the design, assessment, and management of preservation methods for archaeological iron.

While there are many variables that influence the corrosion of archaeological iron, a nuanced scale recording how changing RH affects corrosion rate and its relationship with the Cl^- content of iron objects is central to achieving this goal. To this end, the study reported here uses a unique experimental design, employing a highly accurate and sensitive technique for remotely detecting oxygen concentration, to deliver quantitative data on the corrosion rate of a large number of archaeological iron objects as a function of ambient RH. Further, it relates the Cl^- content of these archaeological objects to their corrosion rate at specific RH values to provide insight into the relationship between the two variables.

The usefulness of such a scale is apparent when considering current approaches to the preservation of archaeological iron. These focus on removing one or more of three essential variables that drive electrolytic corrosion; water, electrolyte, and oxygen. Procedures and techniques used to do this can be either interventive or preventive. Interventive methods largely fall into three categories: the use of coatings to prevent access of oxygen and/or moisture to electrolytes on the surface of the metallic iron; attempts to solvate and remove electrolytes from objects; and impregnation with corrosion inhibiting chemicals (Scott and Eggert 2009; Watkinson 2013). As these methods invariably lack quantitative data to evidence their effectiveness,

CONTACT Nicola J. Emmerson emmersonnj@cf.ac.uk Department of Archaeology & Conservation, School of History, Archaeology & Religion, Cardiff University, Colum Drive, Cardiff CF10 3EU, UK

Information on the data underpinning the results presented here, including how to access them, can be found in the Cardiff University data catalogue at [http://doi.org/10.17035/d.2019.0066664415]

their outcomes are unpredictable and their use remains questionable. Of the preventive environmental control methodologies available, desiccation remains the most advocated and most commonly used technique (Rimmer et al. 2013). It is proven to be effective, provided RH is kept below threshold corrosion values (Watkinson and Lewis 2005a; Thickett and Odlyha 2014), and is cheap and easy to establish. Since the desiccated storage of archaeological iron normally involves no prior treatment of objects to reduce Cl^- within them, it is important to have quantitative understanding of the relationship between storage RH and Cl^- content of objects relative to corrosion rate.

A quantitative scale that relates corrosion rate to ambient RH and to Cl^- content of objects will identify the risks involved when using desiccation to store untreated archaeological iron. If failure to manage desiccated storage results in the threshold RH corrosion value for Cl^- contaminated iron being exceeded, the magnitude of increased risk can be measured as the change in corrosion rate. The severity of the increase can be used to inform management procedures for renewing desiccants. A quantitative corrosion rate scale can also be used to identify RH values where corrosion escalates exponentially and the level of risk becomes unacceptable. Equally, it can be used to identify RH ranges where risk is low. For instance, how much faster do archaeological iron objects corrode at 40% RH, when compared to desiccation below 10% RH? The answer to this may indicate that it is beneficial to allocate resources to controlling the environment to 40% RH, if it is impossible to bear the added expense of setting up and maintaining an RH below 10%. Establishing danger zones where corrosion risk is high is equally important, while there is only a 10% difference between 60 and 70% RH, what is the rate of increase in corrosion between these values? Extending the quantitative data to include the Cl^- in objects makes it possible to address questions such as, how concentrations of 200–400 ppm Cl^- in iron objects impact on their corrosion rate at specified RH values. How does this compare with objects containing 800–1000 ppm Cl^-? Answers will refine the RH corrosion rate scale and further understanding of risk and how best to manage it.

A second publication will follow this experimental study. This will translate corrosion rate into damage to archaeological objects to expand and refine the risk model generated here. A third publication is underway that quantifies the performance of the hardware used to create desiccated environments. This data will determine how the corrosion rate scale can be applied in practice.

Corrosion profiles

During their burial, which often lasts for millennia, archaeological iron objects develop corrosion product layers that normally contain evidence of their original surface and shape. These layers vary in composition but have been categorised generically as comprising a metal core (M), a dense corrosion product layer (DPL), normally of αFeOOH, Fe_3O_4, and γ-Fe_2O_3, and an outer, more porous transformed medium (TM) of iron oxides and incorporated soil particles (Bertholon 2001; Neff et al. 2007; Saheb et al. 2007; Bellot-Gurlet et al. 2009). Since the archaeological record is embedded in corrosion product layers, post-excavation corrosion need not consume all the remaining iron to destroy the heritage value of archaeological iron. The loss of metal by oxidation, the low pH from Fe^{2+} and Fe^{3+} hydrolysis, and the growth of voluminous corrosion products at the metal surface (Loeper-Attia 2007) causes cracking and detachment of corrosion product layers overlying the residual metal core (Turgoose 1982). This damage removes evidence of object shape and eventually produces complete loss of heritage value. Even minor loss of metallic iron may produce catastrophic damage to corrosion layers according to their form, composition, and integrity.

Post-excavation corrosion variables

Chloride

The form of Cl^- within iron objects is crucial for determining its role in corrosion processes. Chloride solutions provide excellent electrolytes. Upon excavation, archaeological iron objects often contain large numbers of Cl^- ions clustered at anode sites on their metal surface (Neff et al. 2005; Loeper-Attia 2007; Réguer, Dillmann, and Mirambet 2007; Saheb et al. 2007; Watkinson 2010; Watkinson and Rimmer 2014), to which they were attracted during burial as charge balance for Fe^{2+} ions generated by oxidation (Turgoose 1982; Watkinson 1983). Iron objects excavated from temperate zone burial environments dry out, with low ambient RH concentrating the Fe^{2+}/Cl^- solution at the metal surface and hydrolysis of Fe^{2+} lowering pH, which favours the formation of akaganéite (βFeOOH) (Neff et al. 2004; Réguer, Dillmann, and Mirambet 2007; Rémazéilles and Refait 2007) via βFe_2OH_3Cl (Saheb et al. 2007). Ferrous chloride ($FeCl_2.4H_2O$) can also form in these conditions but its hygroscopicity prevents its formation in high ambient RH. This leaves Cl^- in solution to act as an electrolyte. While the presence of Fe^{3+} ions is expected upon excavation, to date, no $FeCl_3$ has been reported as occurring on archaeological iron, which may be due to its ability to react with metallic Fe to produce $FeCl_2$. Hydrolysis of Fe^{3+} will result in low pH values and subsequent acid attack on metallic Fe.

βFeOOH is insoluble and has Cl^- retained in its crystal structure and adsorbed on its surface (Mackay 1960; Ståhl et al. 2003). This surface adsorbed Cl^- is highly mobile in water (Réguer et al. 2009; Watkinson and Emmerson 2017) and it makes βFeOOH hygroscopic

(Kaneko and Inouye 1979; Watkinson and Lewis 2005a). The hygroscopicity mobilises surface adsorbed Cl^-, causing it to corrode iron down to 15% RH (Watkinson and Lewis 2005b; Thickett and Odlyha 2014; Watkinson and Emmerson 2017). Solid $FeCl_2.2H_2O$ does not corrode iron but above 20% RH it hydrates to form $FeCl_2.4H_2O$ which supports the corrosion of iron in contact with it (Turgoose 1982; Watkinson and Lewis 2005b) and deliquesces at 55% RH to provide a strong electrolyte. Therefore, it is normally considered necessary to store Cl^- contaminated archaeological iron below 12% RH to prevent it corroding (Watkinson and Lewis 2005a; Thickett and Odlyha 2014). Although low RH storage is proven to prevent corrosion, it is a costly process to institute and maintain. In contrast, completely mineralised iron objects present no corrosion problems post excavation, as their Cl^- diffuses out during burial where it is no longer required as a counter ion following the oxidation of all Fe and conversion of Fe^{2+} to oxides (Watkinson 1983; Watkinson et al. 2013).

Atmospheric moisture and corrosion product layers

Due to the need for electrolytes to support corrosion and the interaction of moisture with chloride bearing corrosion products, RH is the most important post-excavation corrosion driver for archaeological iron. High RH supports the formation of continuous thick water films on the metal surface (de Rooij 1989; Leygraf and Graedel 2000, 11, 283) that solvate Cl^- located there. Even mid-range RH may provide conditions to support corrosion due to the small internal capillary structures of corrosion layers lowering the corrosion threshold humidity, with water condensing at 50% RH in capillaries of 1.5 nm (Garverick 1994). Apart from its direct impact on corrosion rate, temperature influences RH. This is especially problematic when it either fluctuates widely and rapidly or causes large diurnal changes, with falling temperatures at night raising RH.

Hygroscopicity and deliquescence of compounds, other than iron chlorides and βFeOOH, may influence corrosion rate. During burial, solvated Ca^{2+}, Mg^{2+}, and Na^+ ions can enter objects and associate with Cl^-, forming $CaCl_2$, $MgCl_2$, and NaCl as objects dry post excavation. These highly hygroscopic compounds can deliquesce; NaCl at 75.7% RH (25°C) (Tang, Munkelwitz, and Davis 1977) and $MgCl_2.6H_2O$ at 33.2% RH (25°C) (Wexler and Hasegawa 1954). At the lower RH of 67%, water adsorbs onto NaCl producing a 4.5 nm thickness monolayer (Ewing 2005); even at 20% RH, 0.3–2 nm monolayers of water are recorded (Luna et al. 1998). The presence of such hygroscopic compounds would provide moisture to support corrosion at low humidity. However, other than on marine archaeological iron, characterisation of corrosion product layers on iron from terrestrial burial contexts has not reported the presence of these compounds, although they might be expected to occur given the range of solvated ions within most soils.

Corrosion product layers on archaeological iron have been categorised and extensively characterised (Bertholon 2001; Neff et al. 2004, 2007; Saheb et al. 2007) but their morphology and physical properties are largely unstudied despite these variables influencing oxygen and moisture ingress to the metal surface, hence post-excavation corrosion rates (Vega et al. 2007). A thick, compact, and unbroken DPL will hinder diffusion of water vapour to form electrolytes and oxygen supply to cathodes at the metal surface (Vega et al. 2007), whereas minor cracking provides easier routes for their access and an increased corrosion rate (Emmerson and Watkinson 2016). The properties of the corrosion layers are subject to dynamic change as continuing corrosion creates lamination and cracking, with new corrosion products influencing corrosion rates and routes. This can be expected to influence post-excavation corrosion rates and is the subject of a second publication based on the corrosion rate data reported here. Other intrinsic factors influencing corrosion rate include object shape, alloying elements, and the metal surface, which will have a large area due to the pitting and trammelling that results from corrosion during burial. Slag and impurities can act as cathodes, so their composition, quantity, and distribution will generate anodes that influence the location and quantity of Cl^- in an object, due to its role as a counter ion (Rimmer and Wang 2010). This is a complex set of interrelated variables that are difficult to record quantitatively or, in some instances, even detect.

Research aim and objectives

Aim

- Determine the post-excavation corrosion rate of a range of archaeological iron objects as a function of ambient relative humidity and their chloride content to provide a tool for calculating risk as related to RH.

Objectives

- Measure quantitatively the corrosion rate of a statistically significant number of archaeological iron objects at a range of selected RH values using oxygen consumption of individual objects as a proxy for corrosion rate.
- Digest these archaeological objects and determine their chloride ion content then relate this to their oxidation rate.

Experimental

Experimental design

Sample characteristics

Individual archaeological objects were used as test samples and these were either nails or nail fragments

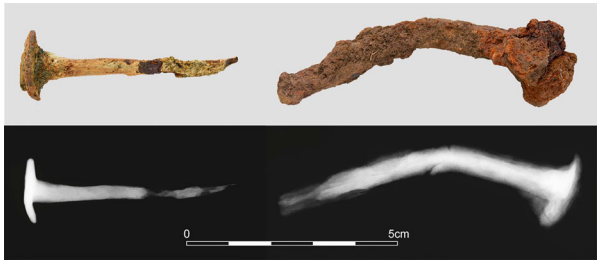

Figure 1. Morphology and radiograph of Billingsgate (left) and Caerleon (right) nail examples.

from the Roman legionary fortress at Caerleon (CPF) in Glamorgan, Wales and the Medieval riverside site of Billingsgate (BWB) in London, England. Metallography of representative nails confirmed these were formed from wrought iron. No information was available on the properties of the burial soils from either site. BWB nails were excavated 18 years previously and CPF nails two years before this experiment. Both groups of nails had been stored with fully desiccated silica gel inside sealed polyethylene boxes to create a dry microclimate to control their corrosion. No maintenance records for the environments were available. While objects with known surface area of metal would offer good standardisation for comparative corrosion testing of the type employed in this study, this is not feasible when using archaeological objects. Nails were chosen because of their similar shape and they were selected to lie within a limited mass range, as this was to be used as a comparator between samples. Radiography confirmed that each nail retained a metallic core, which meant that it was also likely to retain Cl^- ions (Watkinson 1983, 2010; Rimmer et al. 2013; Watkinson et al. 2013).

The two sites had distinct and different corrosion layer morphologies that matched typical generic corrosion profiles (Bertholon 2001; Neff et al. 2007). BWB nails presented a thin, compact, and hard DPL and a fine, thin outer TM layer that represented clearly the shape of the nail, which retained much of its metallic core and showed limited local pitting (Figure 1). CPF nails mostly had a thick corrosion layer with a voluminous, soft, powdery, and porous outer TM layer that obscured object shape. Beneath this was a fairly extensive and uneven DPL that retained the overall shape of the nail and within this was an extensively corroded, pitted metal core (Figure 1). The density of the metallic iron cores makes them the main contributors to object mass for both groups of nails.

Corrosion rates

Oxygen is used in the corrosion of iron and in the transformation of corrosion product compounds. Compounds such as the $\beta Fe_2(OH)_3Cl$, identified as a precursor to the formation of βFeOOH (Neff et al. 2007), may consume oxygen as they transform. Volumetric changes resulting from corrosion product transformations create stresses and pressure on the DPL, causing damage and loss of object integrity. The amount of oxygen consumed both by the oxidation of metallic iron and the transformation of iron corrosion products therefore provides a holistic corrosion rate for archaeological iron as both actions cause damage to the object and this is the effective measure of its corrosion rate in terms of loss in value.

Oxygen consumption of individual objects was measured at a range of static RH values at 20°C over selected time periods. While measuring oxygen consumption does not offer a quantitative value for loss of metallic iron as a function of time, it does provide data for comparing corrosion rates where objects are expected to follow similar oxidation routes in a fixed RH. Corrosion is further standardised by fixed RH within the reaction vessels, avoiding redox reactions that occur in wet/dry corrosion cycles (Hoerlé et al. 2004).

Experimental method

Silica gel conditioning

Silica gel was conditioned to the required test humidities by spreading the gel thinly in trays in a Vötsch VC4018 climatic chamber at 20°C (±0.5°C) with controlled RH (±1%). Conditioning was monitored by placing a 10 g sample of the gel on a Mettler Toledo XS205 balance (±0.00001 g) within the climatic chamber and dynamically recording its mass every 15 min. Full equilibration was achieved when no further mass gain or loss was recorded over a one-week period.

Reaction vessels and oxygen consumption

To measure oxygen consumption, each nail was placed in a polystyrene weighing boat in an individual 250 cm^3 glass reaction vessel with airtight seal. A MadgeTech 101A data logger in each reaction vessel recorded RH (±3%) and temperature (±0.5°C). The appropriate mass of silica gel conditioned to the required test RH was added to the reaction vessel to control its internal RH. A PSt3 oxygen sensor spot (World Precision Instruments (WPI) part #503090), was attached to the inside of each reaction vessel using a transparent RTV silicone rubber (Radio Spares). The reaction vessels were stored in a Binder KBF240 climatic chamber at 20°C (±0.5°C) throughout the test period to control the internal temperature of the reaction vessel to maintain the chosen internal equilibrium RH and avoid temperature sensitive reaction rate changes. Reaction vessels were stored in the climate chamber for 24 h to allow their temperature to reach 20°C and were then opened to equilibrate internal and external pressure before final sealing. Oxygen partial pressure (mbar) within each vessel was measured remotely through the reaction vessel glass using a WPI OxyMini oxygen meter (WPI OXY-MINI-

Table 1. Groups of nails, number, and origin of nails within the group, humidity of the test environments, and the duration of the tests.

	Test 1				Test 2			
Group	RH %	BWB nails	CPF nails	Duration (days)	RH %	BWB nails	CPF nails	Duration (days)
G1	20	12	15	428	30	12	15	332
G2	50	15	15	168	60	15	15	110
G3	80	27	27	80	40	5	15	206
G4	70	8	10	159	–	–	–	–

AOT) and fibre optic cable (WPI cable #501644). The accuracy of the oxygen measurements is ±2 mbar at 210 mbar (atmospheric oxygen pressure) and increases with decreasing oxygen pressure.

Sample groupings

The mass of individual nails was recorded using a Mettler Toledo XS205 balance (±0.00001 g) and groups were created containing both BWB and CPF nails. The oxygen consumption of each nail was monitored at regular intervals over differing time periods (Table 1). Some groups were then either transferred to higher or lower humidity and the oxygen consumption measurement repeated. Frequency of oxygen measurement was influenced by the rate of oxygen consumption; fast consumption rates require more frequent measurement to ensure the slope of the regression line is recorded accurately. For operational reasons, not all nails in G3 included in Test 1 were transferred to Test 2 (Table 1).

Reproducibility and standardisation

To facilitate comparisons between individual nails, standardisation, reproducibility, and error testing was carried out (Emmerson and Watkinson 2014; Watkinson and Rimmer 2014). To assess error and reproducibility when measuring slow corrosion rates over months, it was necessary to determine the long term ingress of oxygen into the reaction vessel and explore whether the vessel contents influenced oxygen concentration or sensor spot accuracy. Eight reaction vessels containing sensor spots were partially filled with nitrogen gas to reduce their internal oxygen pressure and sealed. Oxygen ingress was determined by measuring the partial pressure of oxygen at intervals over 200 days for eight samples and the regression line was recorded (Table 2). Change was within the accuracy of the meter (±2 mbar) indicating minimal or negligible oxygen ingress.

Table 2. Control experiments to determine oxygen ingress. A regression value close to zero indicates a negligible leakage rate.

Sample	Regression line
Nitrogen 1	0.008
Nitrogen 2	0.013
Nitrogen 3	0.014
Nitrogen 4	0.013
Nitrogen 5	0.013
Nitrogen 6	0.015
Nitrogen 7	0.014
Nitrogen 8	0.003

Results of oxygen consumption testing of reaction vessels containing silica gel, weigh boat, and datalogger but no iron sample revealed that no oxygen is consumed by these components of the experimental system at any test humidity (Emmerson and Watkinson 2014; Watkinson and Rimmer 2014). Any oxygen consumed during the tests is attributed to corrosion of the iron objects or transformation of corrosion products within the vessels.

Determination of chloride content in nail samples

After treatment, objects were dried using oven-dry silica gel as a desiccant for at least two weeks. Objects were then placed in 5 M nitric acid and digested at room temperature in screw-top HDPE containers or in beakers covered with either watch glasses or a polyethylene wax film (Parafilm™) to prevent HCl evaporation. The resulting solutions were neutralised with 3 M NaOH solution, filtered to remove the ferrous precipitate, which was rinsed with deionised water, and the filtrate was analysed using the specific ion meter. A control had previously been run. This comprised a nitric acid solution containing iron ions and a known quantity of Cl^-. This was neutralised with NaOH, then filtered and rinsed to remove the precipitate. The Cl^- content of the filtrate was determined to assess whether adsorbed Cl^- was retained by the precipitate.

Chloride ion analysis was carried out using a Radiometer Analytical PHM250 specific ion meter with Hg/$HgSO_4$ reference electrode and a chloride-specific electrode. A four-point calibration using standard sodium chloride (NaCl) solutions was used and checked for accuracy every two hours during measurement periods using known standards. Treatment solutions were neutralised with 5 M nitric acid (HNO_3) and a 0.5 M ammonium acetate/0.5 M acetic acid buffer was added in a 1:10 ratio. All solutions used deionised water, and blank solutions were checked for chloride contamination of the chemicals. The detection limit was 0.5 ppm and accuracy was c.10%. The specific ion meter measurement protocols for the treatment solution and the digestion method were checked for

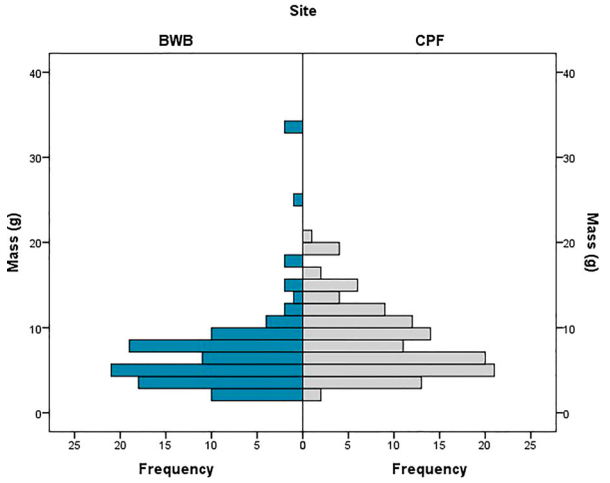

Figure 2. Mass distribution and numbers of nails used in the experimental study.

accuracy and reproducibility using known concentrations of dissolved ferrous chloride.

Results

The mass distribution of the nails used in the experiments is shown in Figure 2. The groups created from these nails, the RH values to which they were exposed, and their duration in these RH test environments are recorded in Table 1 and Figure 3. In some instances, not all nails within a group exposed at the first humidity were transferred to the second humidity value (Table 1).

Oxygen consumption for each object in each RH environment is calculated from the oxygen depletion within individual reaction vessels as oxygen consumption per year related to the mass of the nail it contained (mbar yr^{-1} g^{-1}). When comparing groups of nails, the average oxygen consumption rate (AV mbar yr^{-1} g^{-1}) per group was calculated. In this study, oxygen consumption rate (mbar yr^{-1} g^{-1} and AV mbar yr^{-1} g^{-1}) is used as a proxy corrosion rate.

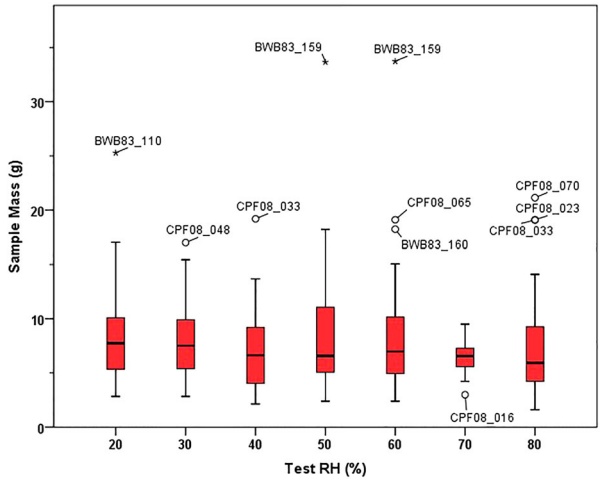

Figure 3. Distribution of object mass within nail groups tested at test RH values.

The various groups were exposed to fixed RH values (Table 1): G1 nails 20% RH followed by 30% RH (Figure 4); G2 nails 50% RH followed by 60% RH (Figure 5); G3 nails 80% RH followed by 40% RH (Figure 6); G4 70% RH (Figure 7). The oxygen consumption ranges of nails comprising groups G1 to G4 are recorded in Figures 8 and 9. Oxygen consumption rates over the test period were all linear.

Results of digesting the nails and determining their Cl^- content are recorded in Figure 10.

Discussion

The data set clearly quantifies how RH impacts on the post-excavation corrosion rate of archaeological iron and identifies generic differences between the corrosion rates of nails from different archaeological sites. Groups of corroded iron nails show similarities between their oxygen consumption rates at the same RH, with increasing RH raising corrosion rate significantly once 50% RH is exceeded. There is a broad ranging trend showing a relationship between increasing Cl^- concentration in nails and rising corrosion rate. However, this trend cannot be used to predict the corrosion rate of an individual iron nail; individual nails having similar Cl^- concentration may consume oxygen at very different rates at the same RH. Variables other than Cl^- concentration must significantly influence corrosion rate as a function of RH. Discussion here centres on the evidence to support these statements, the practical use of the corrosion rate scale produced for the long-term conservation of archaeological iron, and identifying which variables may influence corrosion rate, irrespective of Cl^- content of an object.

Object groups

Mass distribution of the nails from each site confirmed the validity of making comparisons between the sites (Figure 2), as did the mass range within the nail groups created (Figure 3). Oxygen consumed per unit surface area would be the preferred method for studying the corrosion rate of these nails. However, each sample nail has a different mass and surface area, with corrosion product layers of differing density, porosity, and coherence obscuring the uneven trammelled surfaces of their metal cores, consequently it is impossible to record the surface area of metal. The uniqueness of the archaeological samples means that mass is the only readily measurable object comparator.

Similarities exist between the samples, as the original form of each nail was a tapering square section with a flat head, but many nails may now lack either a head or part of their shaft, or both. In their non-corroded state, since volume is related to mass of metal, the generic shape of the nails will produce similar ratios when comparing the volume of metal to its

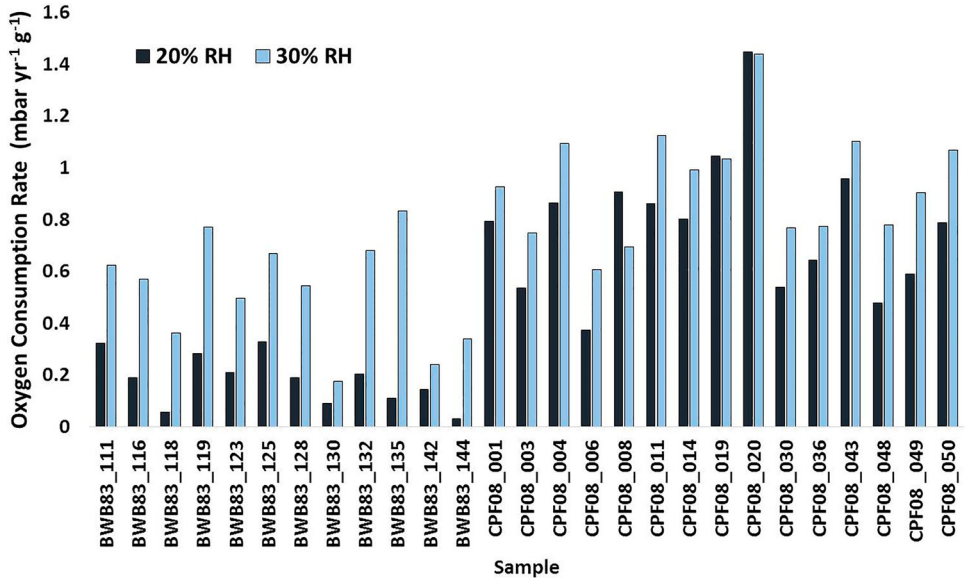

Figure 4. Oxygen consumption rate of nails in group G1 exposed at 20% RH (428 days) followed by 30% RH (332 days).

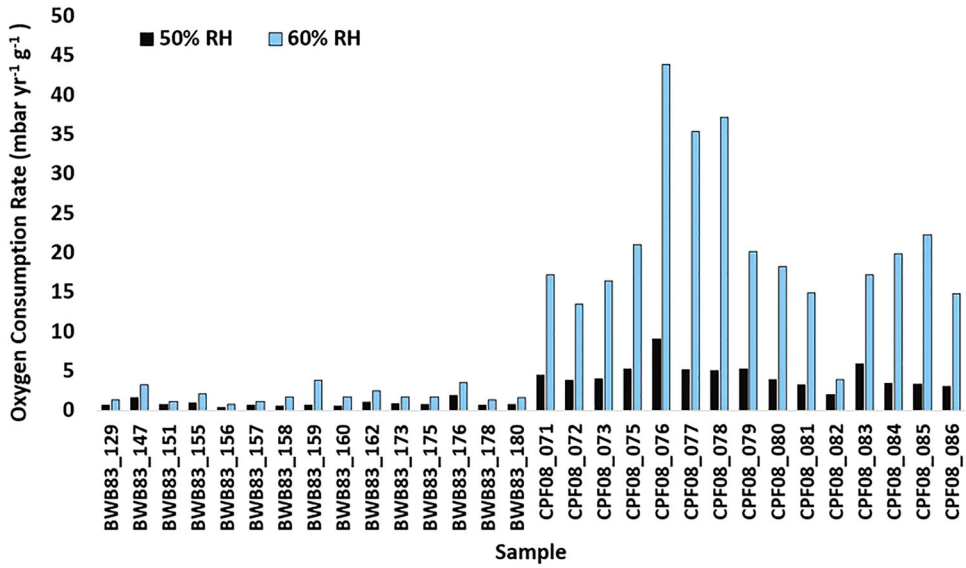

Figure 5. Oxygen consumption rate of nails in group G2 exposed at 50% RH (168 days) followed by 60% RH (110 days).

surface area, even for these hand forged examples. Once the nails corrode extensively, as in this sample set, the mass to surface area relationship will change dynamically and uniquely for each nail.

Despite the corroded condition of the nails, mass appears to remain a useful comparator. Nail samples with greater mass generally consume more oxygen, as their larger surface area offers more scope for establishing anode sites (Figure 11). Also, comparing corrosion rate per gram of nail reveals similarities in rate, irrespective of the overall mass of the nail (Figure 12). This is likely a result of there being no extreme differences between sample surface area, as would occur when comparing objects of similar mass but with differing morphology such as thin sheet and cuboid shapes. Therefore, despite the lack of variable standardisation within the sample set, mass remains the only inter object comparator of use in these tests and the validity of using mass to normalise the data can be seen when comparing Figures 11 and 12.

Oxygen consumption of individual nails

There was a generic difference between the oxygen consumption rates of nails from the two archaeological sites used in these tests. At the same RH values over the range 20–70% RH, nails from Caerleon (CPF) exhibited higher oxygen consumption rates than nails from Billingsgate (BWB) (Figures 4–7) and rate differences at 50% RH were particularly notable (Figure 5). It is likely that the morphology and composition of corrosion product layers on the nails influence corrosion rates. This and the implications for the extent and nature of the damage caused by corrosion are the subjects of a second article reporting this research.

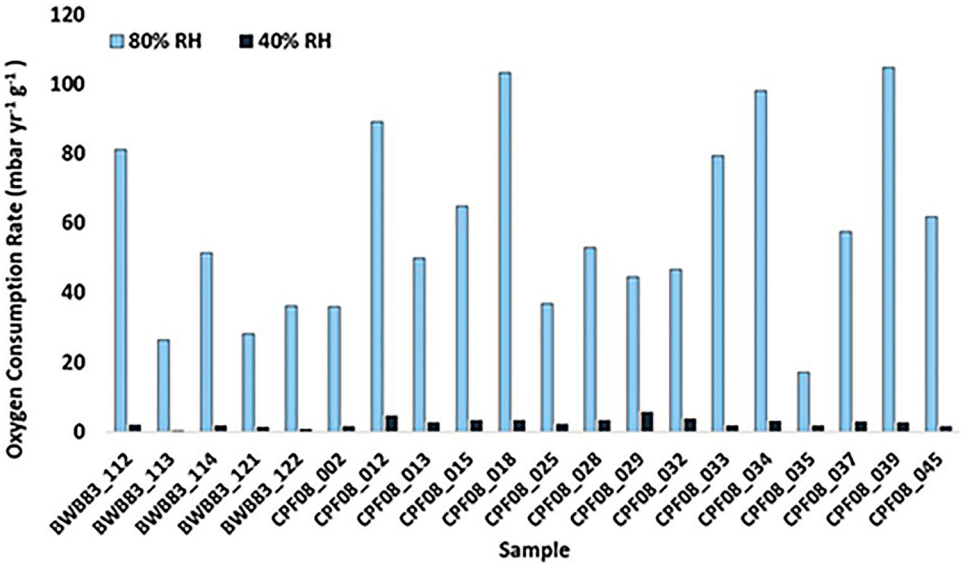

Figure 6. Oxygen consumption rate of nails in group G3 exposed at 80% RH (80 days) followed by 40% RH (206 days).

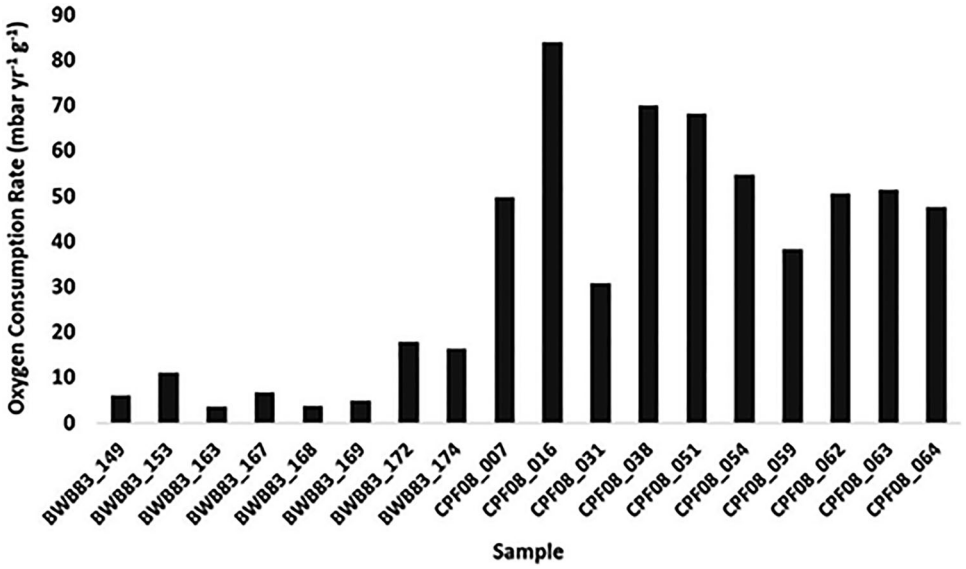

Figure 7. Oxygen consumption rate of nails in group G4 exposed at 70% RH (159 days).

Both CPF and BWB nails recorded very low oxygen consumption rates at 20 and 30% RH (Figure 4). At 30% RH, seven CPF nails had 15–62% increases in their oxygen consumption, two showed no increase, and one anomalously reduced its consumption by 24% (Figure 13).

For G2 nails, exposed first to 50% RH then 60% RH (Table 1), oxygen consumption of both BWB and CPF nails increased significantly at 60% RH (Figures 5 and 14). The greater stability of BWB nails when compared with CPF is reflected in their slower oxygen consumption (Figure 5) and lower percentage consumption rate increases at 60% RH (Figure 14). Compared to the low oxygen consumption range of G1 CPF nails over the 20% RH to 30% RH range (minimum 0.3 and maximum 1.4 mbar yr^{-1} g^{-1}) (Figure 4), G2 CPF nails have a much greater oxygen consumption range at 50 and 60% RH (minimum 2 and maximum 44 mbar yr^{-1} g^{-1}) (Figure 5).

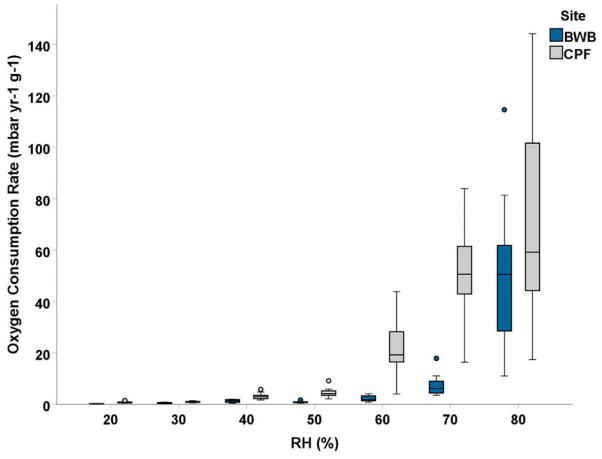

Figure 8. Oxygen consumption of groups of nails at each test humidity compared. BWB83 146 (BWB 80% sample) is an extreme outlier and has been removed from the dataset. Note that oxygen consumption of all G3 nails run at 80% RH is shown, including those not subsequently tested at 40% RH.

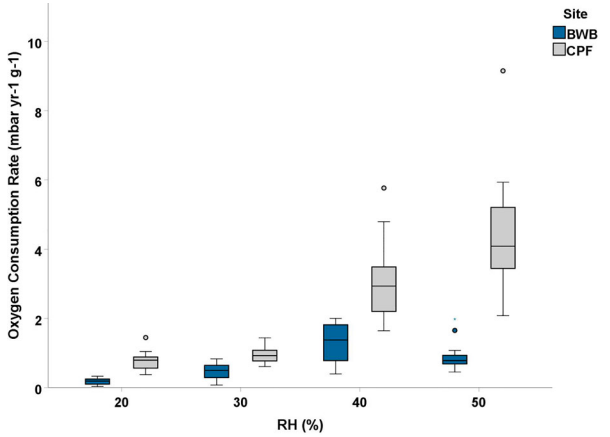

Figure 9. Oxygen consumption of groups of nails within 20–50% RH compared.

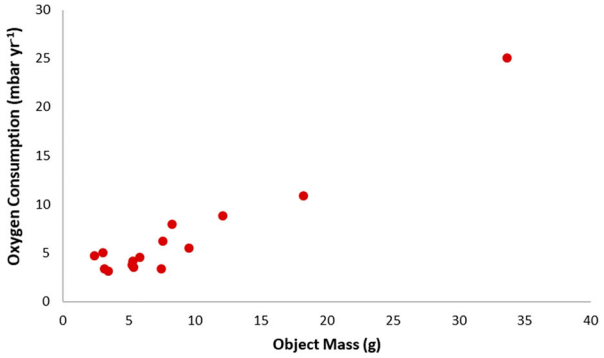

Figure 11. Relationship between oxygen consumption rates (mbar yr^{-1}) and object mass at 50% RH for BWB nails.

Unlike the G1 and G2 double exposure tests, where nails were moved from lower to higher humidity, selected nails in G3 were moved from high (80%) to low (40%) humidity. At 80% RH all nails recorded very high oxygen consumption rates and these reduced significantly at 40% RH (Figure 6). The merit of storing archaeological iron at 40% RH is evidenced by the oxygen consumption of 18 out of 20 nails falling by over 92% (Figure 15).

Oxygen consumption of nail groups: differentiation by site

Comparing nail groups reveals two differing patterns of oxygen consumption according to site origin. CPF nails show an incremental rise in rate from 20 to 80% RH as a function of RH (Figure 8). Increases are small up to 50% RH, where the maximum consumption is <6 mbar yr^{-1} g^{-1} (Figure 9), until escalation begins at 60% RH and rises rapidly through 70–80% RH, where values as high as 144 mbar yr^{-1} g^{-1} occur (Figure 8). Inclusiveness of the oxygen consumption rates of the G4 70% CPF nails within the range of the G3 CPF 80% RH nails reveals extreme instability of CPF at RH values at and above 70% RH (Figure 16). While the higher RH produces some oxygen consumption values above the highest rate recorded at 70% RH, corrosion rates at 80% RH do not necessarily exceed those at 70% for CPF nails. This may indicate that a continuous film of water has been established at 70% RH and that thickening it at 80% RH does not automatically increase corrosion rate but, conversely, could potentially hinder it by offering a longer path for oxygen diffusion to cathode sites.

The BWB oxygen consumption pattern differs, recording very low consumption rates up to and including 60% RH (< 3.2 mbar yr^{-1} g^{-1}) (Figures 8 and 9). The anomalous oxygen consumption rise at 40% RH is potentially misleading; since the group comprised only 5 nails it is not considered statistically representative. Further, there is potential for damage sustained by the corrosion product layers of nails at 80% RH to impact on their oxygen consumption rate at 40% RH. The rapid corrosion that occurs at 80% RH will have caused loss of metal, which produces

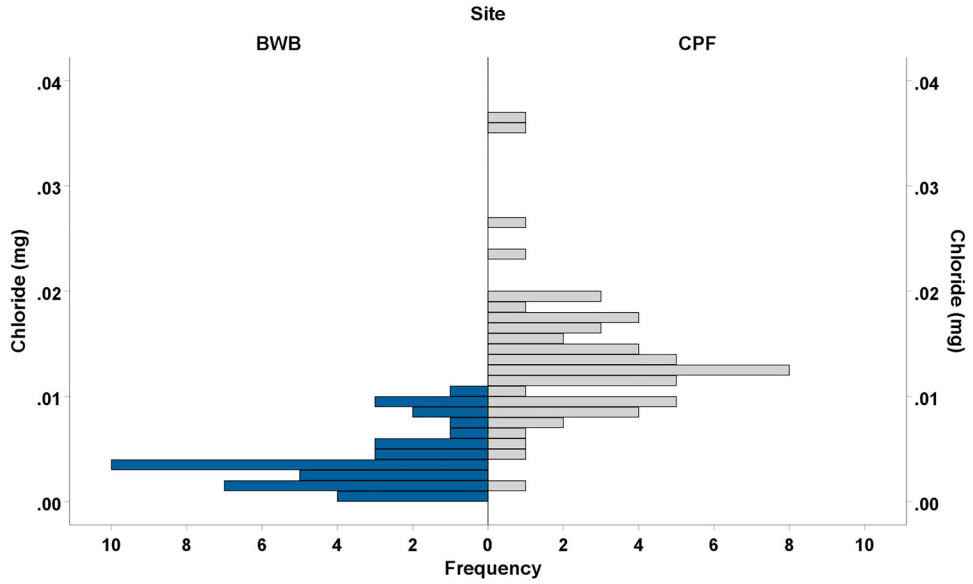

Figure 10. Histogram showing chloride content of the iron nails comprising the sample set from both sites.

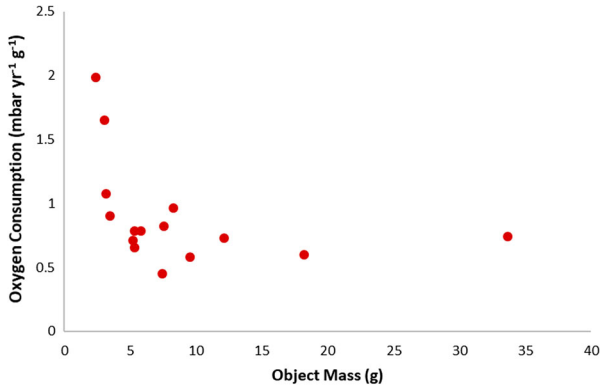

Figure 12. Oxygen consumption rates by mass of object (mbar yr^{-1} g^{-1}) at 50% RH for BWB nails.

Fe^{2+}/Cl^{-} rich solutions in the water film. Dehydration at 40% RH will remove these water films allowing for the ready access of oxygen to the metal surface via new cracks and fissures produced at 80% RH, with subsequent formation of iron oxides involving residual Fe^{2+}, Fe^{3+}, and Cl^{-}. Corrosion of BWB nails escalates at 70% RH but there remains a degree of overlap between oxygen consumption rates of G4 70% RH BWB nails and several G2 BWB nails at 60% RH (Figure 17). While a similar, limited overlap pattern between 80 and 70% RH is evident for G3 BWB oxygen consumption rates, generally there is a notable increase in BWB oxygen consumption at 80% RH as compared to 70% RH (Figures 6–8 and 18).

Differences in the pattern of oxygen consumption between nails from the two sites are reflected by CPF oxygen consumption rates at 70% RH falling within the consumption range of the BWB 80% RH nail group (Figures 8 and 19). There are only two BWB 80% RH outliers consuming more oxygen than the highest consumption by a G3 CPF 70% RH nail (Figure 19). CPF nails are clearly more unstable than BWB nails but at 80% RH, both CPF and BWB nails have high oxygen consumption rates, with a high degree of inclusiveness of BWB corrosion rates in the CPF range (Figure 20). However, examining detail of the distribution of corrosion rates suggests that CPF nails remain more reactive than BWB nails, particularly if the BWB outlier at 225 mbar y^{-1} g^{-1} is not considered (Figure 20).

The increase in oxygen consumption rate above 60% RH is attributable to the formation of water layers on metal surfaces at higher RH (de Rooij 1989; Leygraf and Graedel 2000, 11) that produces electrolytes using intrinsic soluble ions such as Cl^{-}. Nail variables, such as Cl^{-} content, Cl^{-} form, and corrosion layer morphology, may determine the wide range of oxygen consumption rates recorded at 70 and 80% RH. Once a water film is established, which the high rate of oxygen consumption indicates has occurred at 80% RH, corrosion rate would not be expected to change appreciably. The significant change in oxygen consumption, as RH is lowered from 80 to 60%, could be influenced by this being below the deliquescence point of NaCl at 75.5% RH (20°C) (Wexler and Hasegawa 1954), provided this compound is present from ingress during burial in the soil. At 80% RH, its deliquescence would contribute to establishing a film of water. Any fluctuations between 80 and 50% RH would effectively produce a film loss/film gain cycle for archaeological iron, with corrosion rate varying accordingly. Water films also promote physical damage by facilitating Fe^{2+} and Fe^{3+} hydrolysis, which lowers pH to favour dissolution of corrosion product layers and formation of voluminous βFeOOH (Refait and Génin 1997; Leygraf and Graedel 2000, 46), whilst also promoting Askey's acid regeneration cycle (Askey et al. 1993). This results in cracking and exfoliation of the corrosion layers and the weeping at surface cracks and fissures evident on many nails. The nature of this damage and its relationship to RH and Cl^{-} content of objects is the subject of a forthcoming paper.

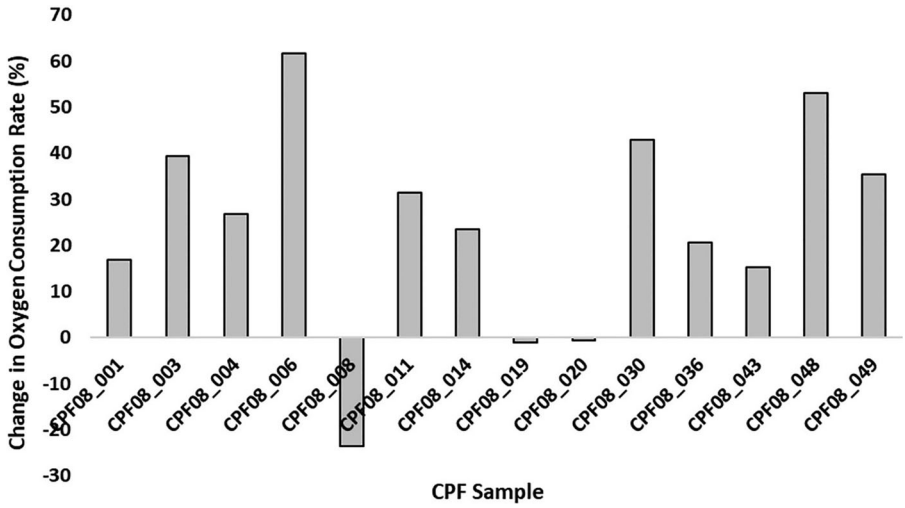

Figure 13. Percentage change in oxygen consumption rates of CPF nails in G1 at 30% RH as compared to 20% RH.

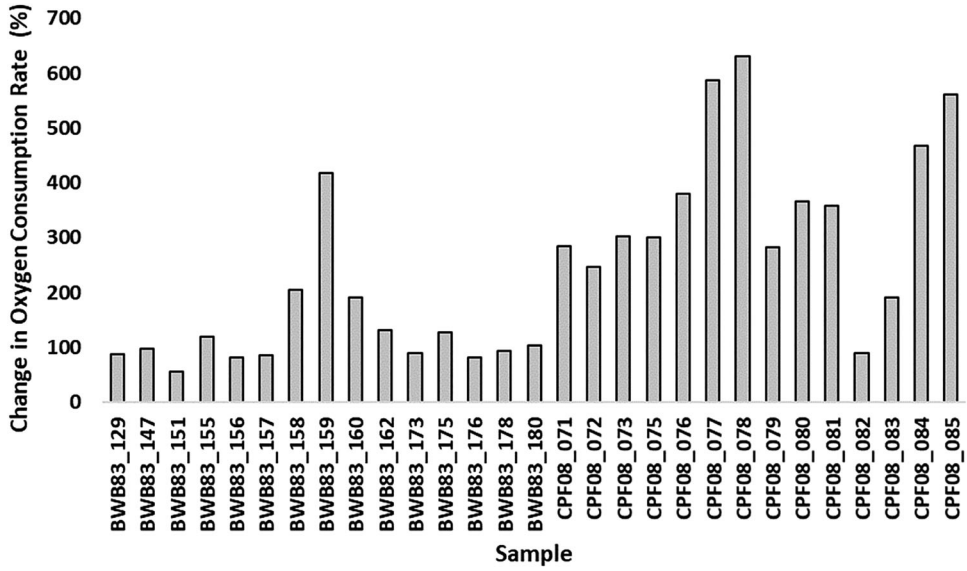

Figure 14. Percentage change in oxygen consumption rates of BWB and CPF nails in G2 at 60% RH as compared to 50% RH.

Chloride content of nails

There are differences between the Cl^- content of nails related to their origin. Nails from the BWB site contain significantly less Cl^- than those from CPF (Figure 10); 8 BWB nails contain 0.005 > 0.01 mg and 30 have <0.005 mg. In contrast to this, 40 CPF nails have >0.01 mg Cl^- and 17 of these contain >0.015 mg Cl^-, whereas only 10 nails contain <0.01 mg Cl^- and 2 of these contain <0.05 g Cl^-. The range of Cl^- concentrations for the CPF site is wide due to outliers (237–4469 ppm), whereas the BWB site has a more limited Cl^- range with few outliers (Figure 21). While the mass of Cl^- does not take into account the mass of the nails, it was established that the mass range of nails from the sites was comparable (Figure 3).

Relating the mass of a nail to its Cl^- content reveals no distinct pattern; nails of similar mass from the same

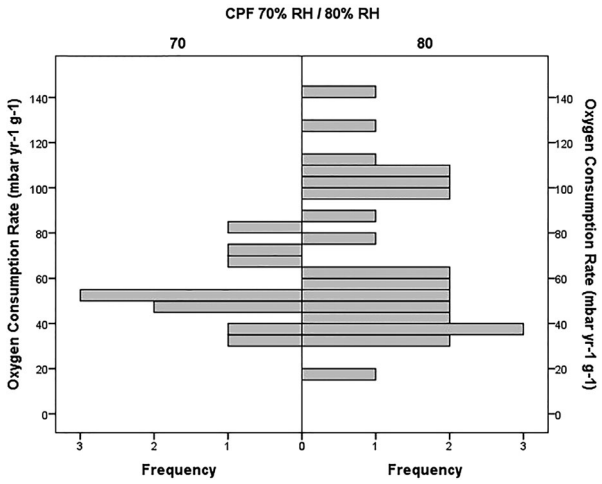

Figure 16. Distribution of oxygen consumption rates for G4 CPF nails at 70% and G3 nails at 80% RH.

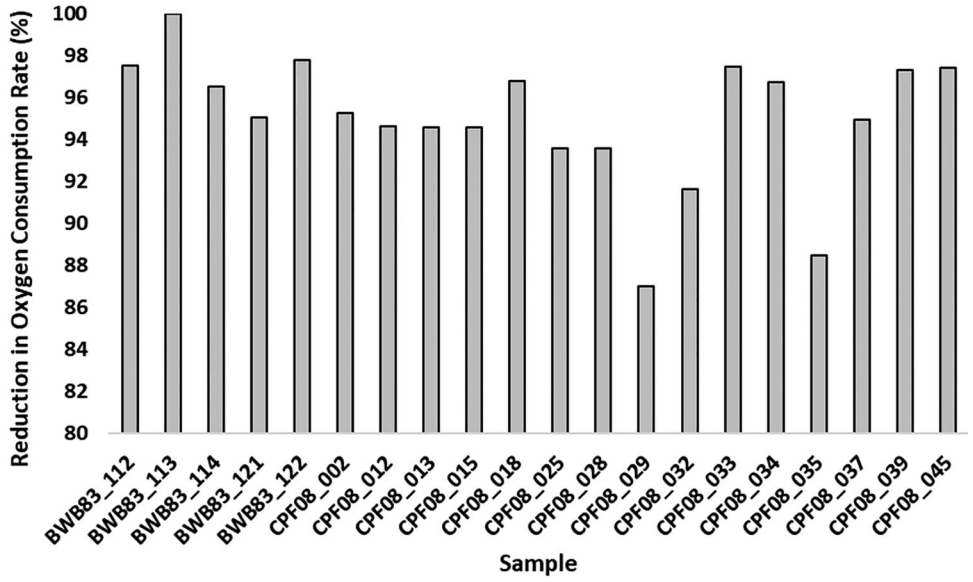

Figure 15. Percentage reduction in oxygen consumption rate of BWB and CPF nails in G3 at 40% RH as compared to 80% RH.

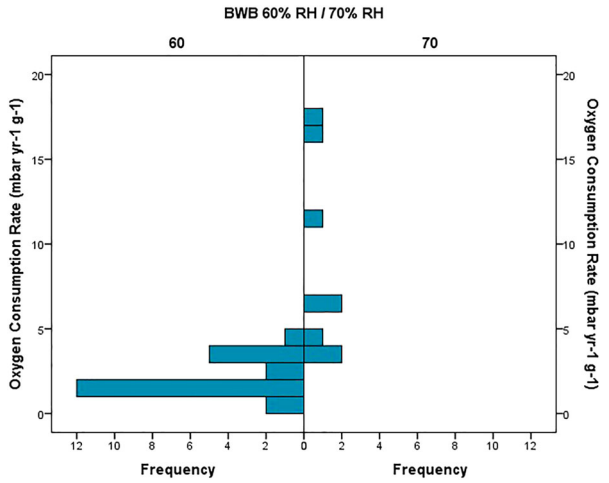

Figure 17. Distribution of oxygen consumption rates for BWB nails at 60 and 70% RH.

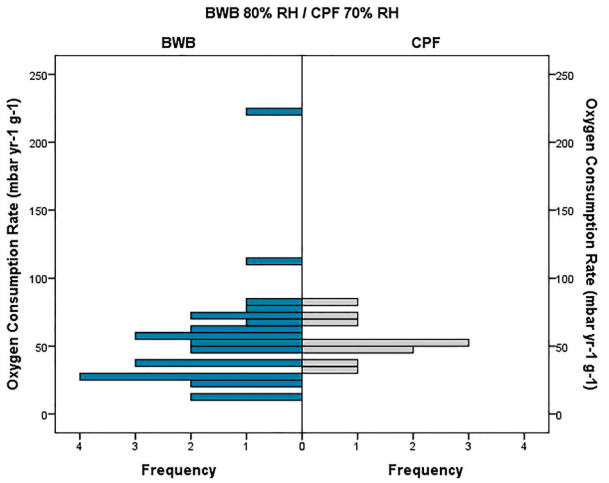

Figure 19. Distribution of oxygen consumption rates for BWB nails at 80% RH and CPF nails at 70% RH.

site can either have virtually the same Cl^- concentration or, in extreme instances, have a difference of several hundred ppm in magnitude (Figure 21). There is no correlation between increasing mass of a nail and its Cl^- content; heavier nails do not have higher Cl^- concentrations than lighter nails or vice-versa (Figure 21). An earlier study revealed that nails retaining a thin slither of metallic iron in an advanced state of corrosion contained more Cl^- than heavier nails from the same archaeological site (Watkinson 1983). This was attributed to active corrosion attracting Cl^- ions to anode sites on the metal surface and concentration build up as corrosion progresses, since the generation of more Fe^{2+} attracts more Cl^- to counterbalance charge in the electrolyte. No verification of this theory can be provided for the samples in the tests here, as there is insufficient data on the degree of mineralisation within the nails.

The concept of higher Cl^- concentrations within archaeological iron producing faster post-excavation corrosion rates is accepted within conservation and is central to assessing corrosion risk. It influences storage design and the development and assessment of treatments that aim to remove Cl^- from iron (Ståhl et al. 2003; Rimmer, Watkinson, and Wang 2013). Data produced in this study aligns with this thinking by offering evidence that higher Cl^- concentrations produce faster corrosion but it also reveals that there are many anomalous data points within the generic trend. While increased corrosion rate (oxygen consumption) correlates with increasing Cl^- content of nails when the BWB and CPF sites are considered together (Figures 22 and 23), there is no correlation when each site is examined individually. Nails that record broadly similar oxygen consumption rates may have different Cl^- concentrations within them, while other nails have similar Cl^- content and similar oxygen consumption rates. For example, at 80% RH CPF nails with 996 and 1216 ppm Cl^- return oxygen consumption rates of 37 and 98 mbar yr^{-1} g^{-1} and two nails with even closer Cl^- concentrations 1457 and 1431 ppm record oxygen consumption values 62

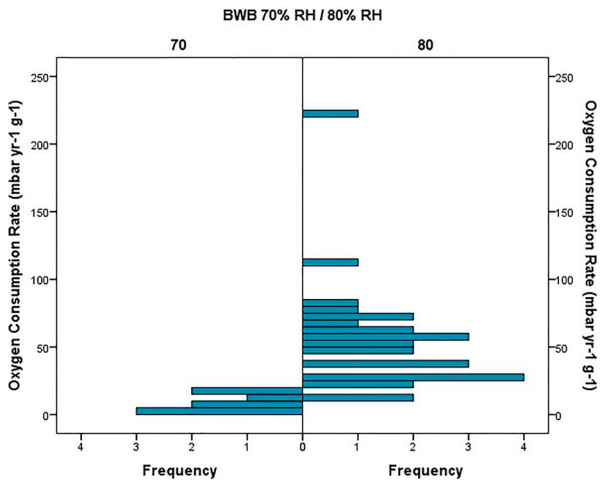

Figure 18. Distribution of oxygen consumption rates for BWB nails at 70 and 80% RH.

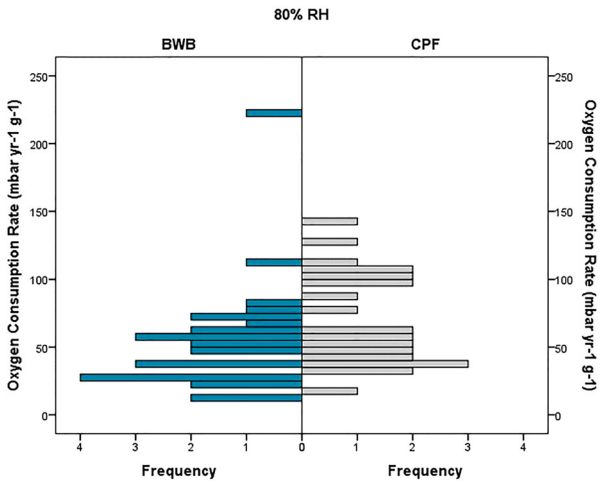

Figure 20. Distribution of oxygen consumption rates for BWB and CPF nails at 80% RH.

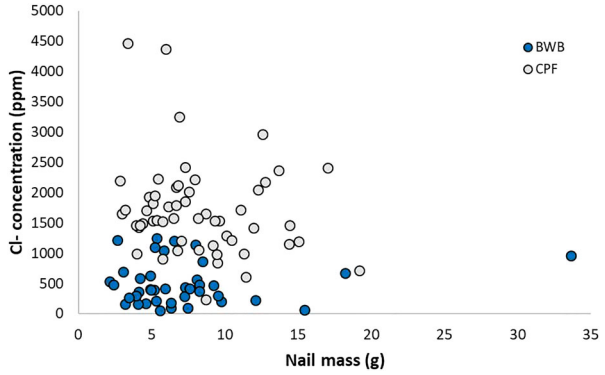

Figure 21. Chloride concentration in BWB and CPF nails.

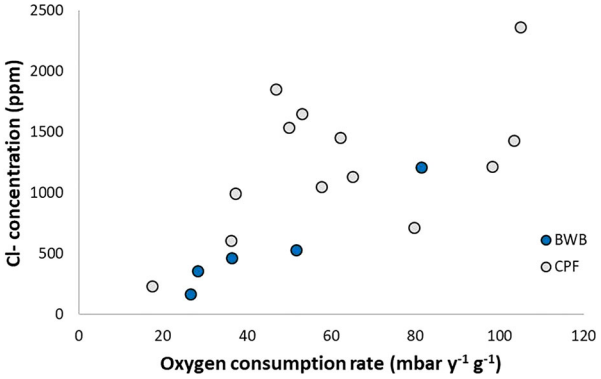

Figure 23. Oxygen consumption of nails exposed at 80% relative humidity as a function of chloride concentration within the nails.

and 103 mbar yr^{-1} g^{-1} at 80% (Figure 23). In addition, a nail may record the same oxygen consumption rate as another nail that has 50–75% more Cl^- within it. At 50% RH two nails with oxygen consumption rates of 0.79 mbar yr^{-1} g^{-1} and 0.78 mbar yr^{-1} g^{-1} have Cl^- concentrations of 217 and 1048 ppm, respectively (Figure 22).

Evidence of a generic correlation between oxygen consumption and Cl^- concentration, when data from both sites are plotted on a single graph (Figures 22 and 23), could be explained by the range of the Cl^- concentrations being more extensive than for a single site. Examining data at 50% RH (Figure 22) shows that there are two distinct Cl^- concentration ranges according to site; 92–1248 ppm for BWB nails and 992–2219 ppm for CPF nails. Combining them provides a full range of Cl^- concentrations from 92 to 2219 ppm with overlap of data sets in the region 950–250 ppm. However, to confirm that there is a correlation between oxygen consumption and Cl^- concentration, all the nails would need to be from the same site. There is no evidence to show that if there were CPF nails with Cl^- concentration <992 ppm they would return similar oxygen consumption data as the BWB nails with Cl^- concentrations in this region. They may continue to produce data that falls within the same oxygen consumption range of 2–9 mbar yr^{-1} g^{-1} as is already occurring for the CPF site (Figure 22).

A different pattern emerges when combining data from both sites at 80% RH (Figure 23). The concentration of Cl^- in nails from BWB lie within the same range as nails from CPF and each site shows increasing oxygen consumption with increasing Cl^- concentration but with a large number of anomalies, where nails of significantly differing Cl^- concentration record similar oxygen consumption rates (Figure 23). However, this is statistically questionable as there are only 5 BWB nails but 12 CPF nails. Despite this difference in numbers of nails, it is worth postulating that this may be a valid correlation. As it is evident at 80% RH, it could be because at this RH there is a distinct film of moisture within the object. This improves the distribution and mixing of the electrolyte and may manifest itself as corrosion that reflects Cl^- concentration. In contrast, at 50% RH there is no film of water, which may mean the impact of Cl^- concentration is different and is perhaps more limited or localised.

Generically, the data here support the expectation that a nail containing high levels of Cl^- will corrode more rapidly than a nail with less Cl^- likely due to increased conductivity of the electrolyte and a greater number of anode sites. Exceptions exist within the data, however, indicating that there is not always a direct correlation between amount of Cl^- and corrosion rates. Variables other than Cl^- concentration are influencing corrosion rate and these may be wide ranging (Table 3).

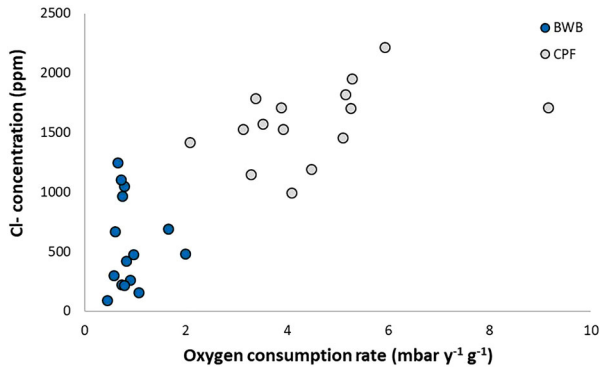

Figure 22. Oxygen consumption of nails exposed at 50% relative humidity as a function of chloride concentration within the nails.

Context of the outcomes for preservation strategies

How can the outcomes of this research influence management procedure and policies? Simple but convincing graphical data, which clearly defines corrosion risk, is often necessary for building evidence-based arguments that will persuade funders to support improved storage or display facilities. To this end, using average oxygen consumption rate to represent corrosion rate can be employed to produce a visual guide for highlighting corrosion risk as a function of RH (Figure 24). At a glance, the catastrophic impact of RH above 60% and the benefits of maintaining RH below 50% RH are clear, with the minor differences

Table 3. Potential reasons why corroded archaeological iron objects with metal cores and similar chloride content may corrode at different rates in the same relative humidity.

Factors	Influences on corrosion
Localisation of chloride	Cl^- may be located in pits whose morphology and geometry makes oxygen access to feed cathode reactions difficult
Chloride widely spread over metal surface and readily accessible	Facilitates large number of cathode and anode sites on the metal surface
Differing corrosion product layers	Morphology, composition, integrity, porosity, thickness and continuity of the corrosion products will affect the ingress of oxygen and moisture to anodes and cathodes
Form of chloride	Highly soluble ferrous chlorides form electrolytes above 60% RH. Surface Cl^- on βFeOOH is soluble. Cl^- occluded in βFeOOH crystal structure does not contribute to corrosion but constitutes part of the Cl^- content of an object
Relative humidity and form of chloride	High relative humidity will solvate soluble Cl^-. βFeOOH can corrode iron as low as 15% RH

between 20 and 30% RH being apparent. While averages (Figure 24) show the similarity between corrosion rates for BWB samples run at 80% RH and CPF samples at 70% RH (Figures 18 and 20), they do not show the extent of overlap between oxygen consumption rates for BWB 70% RH/BWB 80% RH nails and for BWB 80% RH/CPF 80% RH nails evident in detailed data sets (Figures 18–20). Despite these shortcomings, the averages graph clearly defines the impact of high humidity on corrosion rates, demonstrates differences between the corrosion rates of iron from the two sites, and consequently reveals the dangers of expecting all archaeological iron to respond to RH in a similar way.

Results from this study unequivocally reveal that the 'gold standard' for the storage of archaeological iron is below 20% RH, which aligns with other studies that examine aspects of the mechanism of corrosion relative to RH (Ståhl et al. 2003; Watkinson and Lewis 2005a, 2005b; Réguer et al. 2009; Rimmer et al. 2013). By showing clearly that there is little difference in corrosion rate between 30 and 20% RH, the averages graph

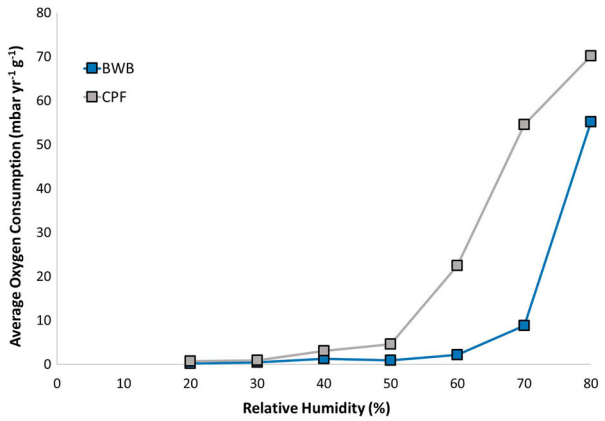

Figure 24. Average oxygen consumption of each nail group as a function of exposure RH and site origin.

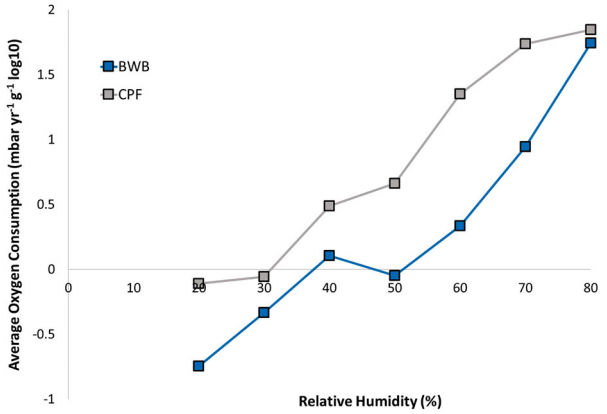

Figure 25. Log of average oxygen consumption of each nail group as a function of exposure RH and site origin.

(Figure 24) offers support for cost benefit calculations where funding is limited and more desiccation equates to greater cost. This is reflected in it showing that a 40% RH environment is significantly beneficial for the longevity of archaeological iron, identifying it as a worthwhile target RH for storage when lower RH values are either too expensive to attain and/or maintain or are not feasible to use when storing mixed materials. As a management tool to persuade funding bodies to support improving storage, Figure 24 offers a convincing argument for maintaining RH values below 40% and preferably 20%. The log scale adopted for Figure 25 clearly identifies the anomalous oxygen consumption rates for both sites at 40% RH, which are thought to be due to the physical integrity of the corrosion products being altered by damage sustained due to prior exposure at 80% RH.

Considering the chloride relationships in this dataset reveals a complex picture, yet one that can inform management procedures. There is confirmation that higher concentrations of Cl^- normally mean faster corrosion rates and that differing sites produce specific and broad Cl^- concentration ranges within objects. At high humidity, low concentrations of Cl^- ($\leq$ 500 ppm) generate rapid corrosion, emphasising the risk posed by Cl^- and supporting the use of treatments designed to lower Cl^- concentration within objects. Unless data is available to demonstrate that Cl^- concentrations in desalinated archaeological iron are reduced to levels where corrosion is negligible, it is necessary to store such iron in the same controlled conditions as untreated iron.

Conclusions

Increasing RH increases the corrosion rate of archaeological iron, which is influenced by Cl^- concentration within objects but not predictably so. It is not possible to say that objects containing higher concentrations of Cl^- corrode faster than those with lower concentrations of Cl^- other than as a generic statement, as

factors other than Cl^- alone are clearly influencing corrosion rate. While storage at or below 20% RH offers what is effectively a no corrosion storage option, corrosion rate differences between 20 and 30% RH are negligible and rise only a little at 40% RH. Controlling RH at 50% remains beneficial for limiting risk, as above 60% RH corrosion accelerates significantly and at 70–80% RH, the lifespan of iron objects measured as their physical integrity, and thus their heritage value, will be very short.

This data provides a management tool for designing cost benefit preservation strategies for archaeological iron based on RH control. Since cost of storage rises as the target RH falls, whether it is as financial outlay to establish desiccated conditions or staff time to maintain them, storage below 40% is identified as beneficial if resources cannot support lower levels of desiccation. Quantifying corrosion rates has offered management a scale for assessing risk and making informed decisions on the benefits of controlling RH to increase the longevity of chloride infested archaeological iron.

Acknowledgements

Iron nails from Billingsgate (London) were kindly provided by Helen Ganiaris at the Museum of London. Nails from Caerleon (Wales) were provided by Dr Peter Guest, Cardiff University.

Disclosure statement

No potential conflict of interest was reported by the authors.

Funding

This work was supported by the Arts and Humanities Research Council/Engineering and Physical Sciences Research Council Science and Heritage Programme [grant number AH/H032754/1 Evidence-based Condition Monitoring Strategy for Preservation of Heritage Iron].

ORCID

David E. Watkinson http://orcid.org/0000-0002-5696-9780
Nicola J. Emmerson http://orcid.org/0000-0001-5277-0865

References

Askey, A., S. B. Lyon, G. E. Thompson, J. B. Johnson, G. C. Wood, M. Cooke, and P. Sage. 1993. "The Corrosion of Iron and Zinc by Atmospheric Hydrogen Chloride." *Corrosion Science* 34: 233–247.

Bellot-Gurlet, L., D. Neff, S. Réguer, J. Monnier, M. Saheb, and P. Dillmann. 2009. "Raman Studies of Corrosion Layers Formed on Archaeological Irons in Various Media." *Journal of Nano Research* 8: 147–156.

Bertholon, R. 2001. "Characterisation and Location of Original Surface of Corroded Metallic Archaeological Objects." *Surface Engineering* 17 (3): 241–245.

de Rooij, A. 1989. "Bimetallic Compatible Couples." *ESA Journal* 13: 199–209.

Emmerson, N., and D. Watkinson. 2014. "Preparing Historic Wrought Iron for Protective Coatings: Quantitative Assessment to Produce Evidence Based Protocols." In *Metal 2013: Interim Meeting of the International Council of Museums Committee for Conservation Metal Working Group, Edinburgh, Scotland 16–20 September 2013*, edited by E. Hyslop, V. Gonzalez, L. Troalen, and L. Wilson, 119–128.

Emmerson, N. J., and D. E. Watkinson. 2016. "Surface Preparation of Historic Wrought Iron: Evidencing the Requirement for Standardisation." *Materials and Corrosion* 67 (2): 176–189.

Ewing, G. E. 2005. "H_2O on NaCl: From Single Molecule, to Clusters, to Monolayer, to Thin Film, to Deliquescence." *Structure and Bonding* 116: 1–25.

Garverick, L. 1994. *Corrosion in the Petrochemical Industry*. 2nd ed. Metals Park, OH: ASM International.

Hoerlé, S., F. Mazaudier, P. Dillmann, and G. Santarini. 2004. "Advances in Understanding Atmospheric Corrosion of Iron. II. Mechanistic Modelling of wet–dry Cycles." *Corrosion Science* 46: 1431–1465.

Kaneko, K., and K. Inouye. 1979. "Adsorption of Water on FeOOH as Studied by Electrical Conductivity Measurements." *Bulletin of the Chemical Society of Japan* 52 (2): 315–320.

Leygraf, C., and T. Graedel. 2000. *Atmospheric Corrosion*. Chichester: Wiley.

Loeper-Attia, M. A. 2007. "A Proposal to Describe Reactivated Corrosion of Archaeological Iron Objects." In *Corrosion of Metallic Heritage Artefacts: Investigation, Conservation and Prediction of Long-term Behaviour*, edited by P. Dillmann, G. Beranger, P. Piccardo, and H. Matthiesen, 190–202. Cambridge: Woodhead.

Luna, M., F. Rieutord, N. A. Melman, Q. Dai, and M. Salmeron. 1998. "Adsorption of Water on Alkali Halide Surfaces Studied by Scanning Polarization Force Microscopy." *The Journal of Physical Chemistry A* 102: 6793–6800.

Mackay, A. L. 1960. "Beta-ferric Oxyhydroxide." *Mineralogical Magazine* 32: 270–280.

Neff, D., P. Dillmann, L. Bellot-Gurlet, and G. Beranger. 2005. "Corrosion of Iron Archaeological Artefacts in Soil: Characterisation of the Corrosion System." *Corrosion Science* 47 (2): 515–535.

Neff, D., S. Reguer, L. Bellot-Gurlet, P. Dillmann, and R. Bertholon. 2004. "Structural Characterisation of Corrosion Products on Archaeological Iron: An Integrated Analytical Approach to Establish Corrosion Forms." *Journal of Raman Spectroscopy* 35: 739–745.

Neff, D., E. Vega, D. Dillmann, M. Descotes, L. Bellot-Gurlet, and G. Béranger. 2007. "Contribution of Iron Archaeological Artefacts to the Estimation of Average Corrosion Rates and the Long Term Corrosion Mechanisms of low Carbon Steel." In *Corrosion of Metallic Heritage Artefacts: Investigation, Conservation and Prediction of Long-Term Behaviour*, edited by P. Dillmann, G. Beranger, P. Piccardo, and H. Matthiesen, 41–74. Cambridge: Woodhead.

Refait, Ph., and J.-M. R. Génin. 1997. "The Mechanisms of Oxidation of Ferrous Hydroxychloride β-$Fe_2(OH)_3Cl$ in Aqueous Solution: The Formation of Akaganeite vs Goethite." *Corrosion Science* 39: 539–553.

Réguer, S., P. Dillmann, and F. Mirambet. 2007. "Contribution of Local and Structural Characterisation Studies of the Corrosion Mechanisms Related to the Presence of Chloride on Archaeological Ferrous Objects." In *Corrosion of Metallic Heritage Artefacts: Investigation, Conservation and Prediction of Long-term Behaviour*, edited by

P. Dillmann, G. Beranger, P. Piccardo, and H. Matthiesen, 170–202. Cambridge: Woodhead.

Réguer, S., F. Mirambet, E. Dooryhee, J.-L. Hodeau, P. Dillmann, and P. Lagarde. 2009. "Structural Evidence for the Desalination of Akaganeite in the Preservation of Iron Archaeological Objects, Using Synchrotron X-ray Powder Diffraction and Absorption Spectroscopy." *Corrosion Science* 51: 2795–2802.

Rémazéilles, C., and P. Refait. 2007. "On the Formation of β-FeOOH (Akaganéite) in Chloride-Containing Environments." *Corrosion Science* 49: 844–857.

Rimmer, M., D. Thickett, D. Watkinson, and H. Ganiaris. 2013. *Guidelines for the Storage and Display of Archaeological Metalwork*. Swindon: English Heritage. http://www.english-heritage.org.uk/publications/guidelines-storage-display-archaeological-metalwork/Storage_Display_Metalwork_2ndPP.pdf.

Rimmer, M., and Q. Wang. 2010. "Assessing the Effects of Alkaline Desalination Treatments for Archaeological Iron Using Scanning Electron Microscopy." *British Museum Technical Research Bulletin* 4: 79–86.

Rimmer, M., D. Watkinson, and Q. Wang. 2013. "The Impact of Chloride Desalination on the Corrosion Rate of Archaeological Iron." *Studies in Conservation* 58 (4): 326–337.

Saheb, M., D. Neff, P. Dillmann, and H. Matthiesen. 2007. "Long Term Corrosion Behaviour of low Carbon Steel in Anoxic Soils." In *Metal 07: Book 2: Innovative Investigation of Metal Artifacts, Interim Meeting of the ICOM-CC Metal WG Amsterdam, 17–21 September, 2007*, edited by C. Degrigny, R. Van Langh, I. Joosten, and B. Ankersmit, 69–75. Amsterdam: Rijksmuseum.

Scott, D., and G. Eggert. 2009. *Iron and Steel in Art: Corrosion, Colourants and Conservation*. London: Archetype.

Ståhl, K., K. Nielsen, J. Jiang, B. Lebech, J. C. Hanson, P. Norby, and J. van Lanschot. 2003. "On the Akaganéite Crystal Structure, Phase Transformations and Possible Role in Post-Excavational Corrosion of Iron Artifacts." *Corrosion Science* 45: 2563–2575.

Tang, I. N., H. R. Munkelwitz, and J. G. Davis. 1977. "Aerosol Growth Studies—II. Preparation and Growth Measurements of Monodisperse Salt Aerosols." *Journal of Aerosol Science* 8: 149–159.

Thickett, D., and M. Odlyha. 2014. "The Formation and Transformation of Akaganéite." In Metal 2013: Interim Meeting of the International Council of Museums Committee for Conservation Metal Working Group, Edinburgh, Scotland 16–20 September 2013, edited by E. Hyslop, V. Gonzalez, L. Troalen, and L. Wilson, 103–109.

Turgoose, S. 1982. "Post Excavation Changes in Iron Antiquities." *Studies in Conservation* 27: 97–101.

Vega, E., P. Dillmann, P. Beranger, and P. Fluzer. 2007. "Species Transport in the Corrosion Products of Ferrous Archaeological Analogues: A Contribution of Modelling of Long-term Iron Corrosion Mechanisms." In *Corrosion of Metallic Heritage Artefacts: Investigation, Conservation and Prediction of Long-term Behaviour*, edited by P. Dillmann, G. Beranger, P. Piccardo, and H. Matthiesen, 92–108. Cambridge: Woodhead.

Watkinson, D. 1983. "Degree of Mineralisation: Its Significance for the Stability and Treatment of Excavated Ironwork." *Studies in Conservation* 29: 85–90.

Watkinson, D. 2010. "Measuring Effectiveness of Washing Methods for Corrosion Control of Archaeological Iron: Problems and Challenges." *Corrosion Engineering, Science and Technology* 45 (5): 400–406.

Watkinson, D. E. 2013. "Conservation, Corrosion Science and Evidence-based Preservation Strategies for Metallic Heritage Artefacts." In *Corrosion and Conservation of Cultural Heritage Metallic Artefacts European Federation of Corrosion No. 65*, edited by P. Dillmann, D. Watkinson, E. Angelini, and A. Adriens, 9–36. Cambridge: Woodhead.

Watkinson, D. E., and N. J. Emmerson. 2017. "The Impact of Aqueous Washing on the Ability of βFeOOH to Corrode Iron." *Environmental Science and Pollution Research* 24 (3): 2138–2149.

Watkinson, D., and M. R. T. Lewis. 2005a. "The Role of βFeOOH in the Corrosion of Archaeological Iron." In Materials Issues in Art and Archaeology VII, Material Research Society Symposium Proceedings 852, edited by P. B. Vandiver, J. L. Mass, and A. Murray, 001.6, Warrendale, PA.

Watkinson, D., and M. T. Lewis. 2005b. "Desiccated Storage of Chloride-contaminated Archaeological Iron Objects." *Studies in Conservation* 50: 241–252.

Watkinson, D., and M. Rimmer. 2014. "Quantifying Effectiveness of Chloride Desalination Treatments for Archaeological Iron Using Oxygen Measurements." In Metal 2013: Interim Meeting of the International Council of Museums Committee for Conservation Metal Working Group, Edinburgh, Scotland 16–20 September 2013, edited by E. Hyslop, V. Gonzalez, L. Troalen, and L. Wilson, 95–101.

Watkinson, D., M. Rimmer, Z. Kasztovszky, Z. Kis, B. Maróti, and L. Szentmiklósi. 2013. "The Use of Neutron Analysis Techniques for Detecting the Concentration and Distribution of Chloride Ions in Archaeological Iron." *Archaeometry* 56 (5): 841–859.

Wexler, A., and S. Hasegawa. 1954. "Relative Humidity-temperature Relationships of Some Saturated Salt Solutions in the Temperature Range 0°C to 50°C." *Journal of Research of the National Bureau of Standards* 53 (1): 19. Research Paper 2512.